PCCP

Accepted Manuscript

ROYAL SOCIETY OF CHEMISTRY

www.rsc.org/pccp

Stability Electronic and Electron Transport properties of Atomic wires anchored on the MoS_2 monolayer

Ashok Kumar[1,2], Douglas Banyai[1],P. K. Ahluwalia[2], Ravindra Pandey[1*],and Shashi P. Karna[3]

[1]*Department of Physics, Michigan Technological University, Houghton, Michigan 49931, USA*
[2]*Department of Physics, Himachal Pradesh University, Shimla 171005, India*
[3]*US Army Research Laboratory, Weapons and Materials Research Directorate, ATTN: RDRL-WM, Aberdeen Proving Ground, MD 21005-5069, U.S.A.*

(July 28, 2014)

*Corresponding author:

Ravindra Pandey (pandey@mtu.edu)

Abstract

Stability, electronic structure, and electron transport properties of metallic monoatomic wires anchored on the MoS_2 monolayer are investigated within density functional theory method. Anchoring of the atomic wires on the semiconducting monolayer dramatically modifies its electronic properties; metallic character of the assembled monolayers appears in density of states and band structure of the system. We find that Cu, Ag and Au wires induce the so-called n-type doping effect whereas Pt wire induce p-type doping effect in the monolayer. The distinctly different behavior of Pt/MoS_2 with the rest of the metallic wires is reflected in the calculated current-voltage characteristics of the assembled monolayers with a highly asymmetric behavior of the out-of-the-plane tunneling current with respect to the polarity of the external bias. The results of the present study are likely to extend the functionality of the MoS_2 monolayer as a candidate material for the novel applications in the areas of catalysis and optoelectronic devices.

Keywords: MoS_2, Density functional theory, Electronic Structure, Density of States, STM

1. Introduction

Two-dimensional molybdenum disulfide (MoS_2) has received considerable attention [1-8] since its synthesis by the exfoliation technique [9] similar to one which was applied to graphene. At ambient conditions, the bulk MoS_2 has a hexagonal structure with the space group of *P63/mmc* [10, 11] in which a layer of Mo atoms is sandwiched between two layers of S atoms. This atomic trilayer configuration is referred to as a monolayer [11]. The atoms within the MoS_2 monolayer are bonded covalently, while individual atomic sheets are bonded via a weak van der Waals force. While the bulk MoS_2 is a semiconductor with an indirect gap, the monolayer has a direct gap [12-14]. Monolayers of MoS_2 have versatile and tunable properties [15-17]which are useful for applications in nanoelectronics [2, 18]. They also complement graphene in applications requiring thin transparent semiconductors, and are expected to have excellent gas sensing performance due to high surface-to-volume ratio [19, 20].

Fabrication of electronic devices for the next generation applications generally requires a combination of conducting and insulating materials by which higher performance and greater flexibility can be achieved [21-25]. For example, Ag nanowires deposited on graphene led to significant enhancement of the conductivity of the functionalized graphene. Consequently, the Ag/graphene system has a greater potential in the high performance, flexible energy conversion and storage devices [21]. Likewise, incorporation of Au nanoparticles on MoS_2 by chemical and microwave route resulted in significant modulation of its electrical and thermal conductivity. The Au/MoS_2 device showed nearly 9-fold increase in the effective gate capacitance, a low Schottky barrier (~14.5 meV) and increase in its thermal conductivity (~23 W/mK) [22]. Considering these experimental results, we are intrigued by the role played by the metallic nanostructures in modifying the electronic properties of a monolayer substrate. Does the effect solely come from nanostructures or the interfacial chemistry of the nanostructure with monolayer play a dominant role? Specifically, we will focus on the monoatomic wires of Cu ($4s^1\ 3d^{10}$),

Ag($5s^1\ 4d^{10}$), Au ($6s^1\ 5d^{10}$) and Pt ($6s^1\ 5d^9$) anchored on the MoS_2 monolayer, and will calculate their stability and electronic properties using density function theory (DFT). Note that the metallic monoatomic wires including Ag, Au and Pt have been synthesized in the break junction experiments and on the substrate [26-29]. The results of the present study are expected to extend the functionality of the MoS_2 monolayer as a candidate material for the novel applications in the areas of catalysis and optoelectronic devices.

2. Computational Methods

Electronic structure calculations were performed within the generalized gradient approximation (GGA) with the Perdew-Burke-Ernzerhof (PBE) parameterization of the exchange and correlation functional form. The norm-conserving, relativistic pseudopotentials [30] as implemented in the SIESTA program package[31] were used in a fully separable non-local Kleinman and Bylander form to treat electron-ion interactions. The Kohn-Sham orbitals were expanded in a linear combination of numerical pseudo-atomic orbitals using split-valance double-zeta with polarization (DZP) basis sets for all atoms. The MoS_2 monolayer, atomic wire and wire/monolayer systems were simulated in the xy plane using the supercell approximation and periodic boundary conditions. A vacuum distance of 15 Å along the z-direction was used to ensure that the negligible interactions between 2D system images. All calculated equilibrium configurations are fully relaxed, with residual forces smaller than 0.01 eV/Å.

3. Results and discussion

3.1 Structural properties

For the pristine MoS_2 monolayer, the calculated lattice constant is 3.23 Å, and the values for the Mo-S bond length and S-Mo-S bond angle are 2.47 Å and 82^0, respectively. These GGA-PBE values are in excellent agreement with the previously reported calculations on the pristine

monolayer [12-14]. Note that the structural configuration of the MoS_2 monolayer shows location of each Mo atom to be at the center of a trigonal prismatic cage formed by six S atoms.

The calculated lattice constants of the monoatomic linear wires of Cu, Ag, Au and Pt are 2.42, 2.65, 2.60 and 2.50Å, respectively. Employing the projected augmented wave (PAW) method, the GGA-PBE values of 2.33, 2.68, 2.61 and 2.35 Å for Cu, Ag, Au and Pt monoatomic wires, respectively were previously reported [32]. A difference of about 6% in the value of lattice constant of Pt may be due to the nature of pseudopotentials used in the PAW method, since the norm-conserving, relativistic pseudopotentials were used to represent the core orbitals for Pt in our study. Moreover, Pt is different from the other noble-metal wires considered in terms of the valance electronic configuration, which may have different dependence of pseudopotential parameters in the theoretical methods, such as the choice of cut-off radius; choice of semicore states; non-linear exchange correlation correction for core-valance electrons interaction etc.

Due to lattice mismatch between the monolayer and monoatomic wires (Table 1), we need to minimize the strain at the interface by a suitable choice of the supercell simulating the assembled monolayer. Our choice of (5x1) supercell of the atomic wire with the (4x4) supercell of the monolayer leads to mismatch of about 6.3%, 2.5%, 0.6% and 3.3% for the co-periodic lattices of Cu/MoS_2, Ag/MoS_2, Au/MoS_2, and Pt/MoS_2, respectively. Here, we define the lattice mismatch to be difference in the calculated lattice parameters of (5x1) atomic wire and (4x4) monolayer. For a specific case of Cu/MoS_2, we have also considered (4x1) supercell of Cu wire together with (3x3) supercell of monolayer which yields the mismatch of 0.1% for the co-periodic lattice of the wire/monolayer system. In this way, the role of the interfacial strains in modifying the electronic properties of the assembled monolayer can be investigated [see supplementary section [33, Figures S1, S2 and S3 in supplementary section].

Alignment of atomic wires deposited on surface of the MoS_2 monolayer can be considered via either top site or hollow site; the former is referred to the case where metal atoms are directly on top of S atoms and the latter is referred to the case where metal atoms are positioned between the two S atoms, thus directly above the underlying Mo atoms of the monolayer (Fig. 1).

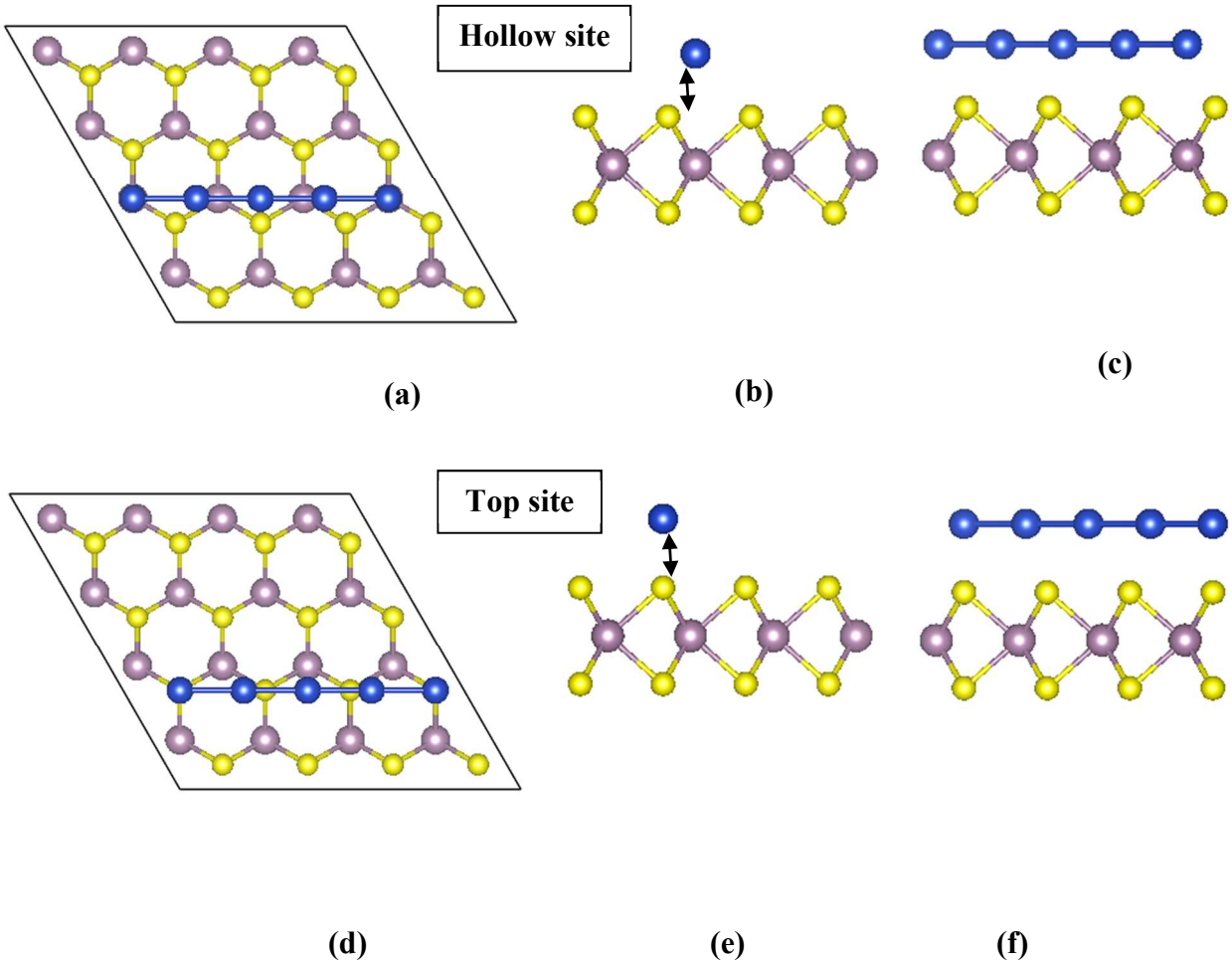

Figure 1: (5x1) monoatomic wires on (4x4) MoS_2 monolayer: (a-c) top and side views of the hollow site, (d-f) top and side views of the top site. The brown, yellow, and blue circles represent Mo, S and atoms of the metallic wires, respectively.

The preferred binding site was determined by performing total energy calculations of the assembled monolayer varying separation between the wire and the monolayer for both top and hollow sites. The binding energy of the assembled system is defined with respect to the constituent components, i.e. $E_b=(EMoS_2+E_{wire}) - (E_{wire}/MoS_2)$. A positive value of E_b indicates stability of the assembled system.

The calculated results are listed in Table 1 showing that difference in E_b of the hollow and top sites for Cu, Ag and Au is small, though the hollow site is slightly preferred over the top site ($\Delta E \approx 0.02$ eV). On the other hand, Pt definitely prefers the top site of the MoS_2 monolayer. The predicted order of stability at the top site is Pt > Cu > Ag ≈ Au for the assembled monolayers. Interestingly, calculations performed at the GGA-PBE level of theory on the diatomic molecules find the binding energy/per atom of 2.39, 2.15, 1.86, and 1.94 eV for PtS, CuS, AgS and AuS molecules, respectively. Therefore, the nature of bonding at the molecular level seems to persist for the wire/monolayer system.

Table 1: The calculated (average) distance between wire and monolayer ($\mathbf{R_{wire\text{-}layer}}$), and the binding energy ($\mathbf{E_b}$) of the assembled monolayer.

System	$R_{wire\text{-}layer}$(Å)	E_b(eV/atom)	
		Hollow site	Top site
Cu/MoS_2	2.3	0.34	0.32
Ag/MoS_2	2.8	0.14	0.12
Au/MoS_2	2.8	0.15	0.13
Pt/MoS_2	2.1	0.34	0.51

3.2 Electronic structure

In order to gain further insight into strength of the interaction between metallic atomic wire with the MoS_2 monolayer, we analyze the charge density difference profile (i.e. $\Delta\rho=$

$\rho_{MoS2+wire}-(\rho_{MoS2}-\rho_{wire})$) shown in Fig. 2. Here, the red region represents the charge accumulation, while the green region represents the charge depletion in the assembled monolayers. We find the MoS2 monolayer to be polarized, and the induced polarization is relatively large for Pt/MoS_2 relative to the other assembled monolayers. This correlates well with the calculated equilibrium separations given in Table 1; the separation between the Pt wire and monolayer is much smaller than the corresponding separation in the other wire/monolayer systems. Following Fig. 2, the predicted order of stability (i.e. Pt > Cu > Ag ≈ Au) is predicted to be directly associated with the degree of polarization induced by wires in the assembled systems.

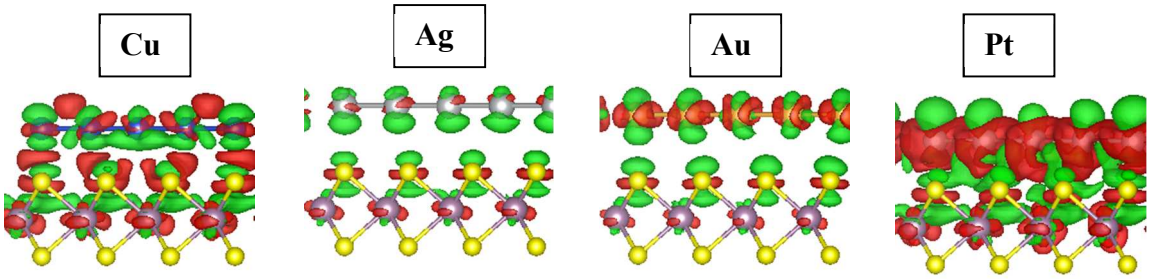

Figure 2: A side view of the charge density difference contour plots. The red (green) regions correspond to accumulation (depletion) regions of the charge density in the assembled monolayers. The contour density is with 0.001 e/Å^3

Analysis of Mulliken charges shows that the monoatomic wires except Pt transfer a fractional charge of ~ 0.05 e/atom to the monolayer, whereas Pt wire gains a fractional charge of ~0.25e from the monolayer. The spatially extended frontier orbitals of Pt which are partially occupied appear to interact strongly with the monolayer following the scenario that was predicted for the PtS molecule. The GGA-PBE calculations on diatomic molecules show that S gives a fractional charge to Pt in PtS whereas Cu/Ag/Au transfers a fractional charge to S in other molecules. Note that the electronegativity difference between Mo (2.16) and S (2.58) atoms induces a fractional charge transfer of 0.3e/atom from Mo to S atoms in the pristine monolayer.

Thus, Cu, Ag and Au wires induce the so-called n-type doping effect, and Pt wire induces p-type doping effect in the MoS2 monolayer.

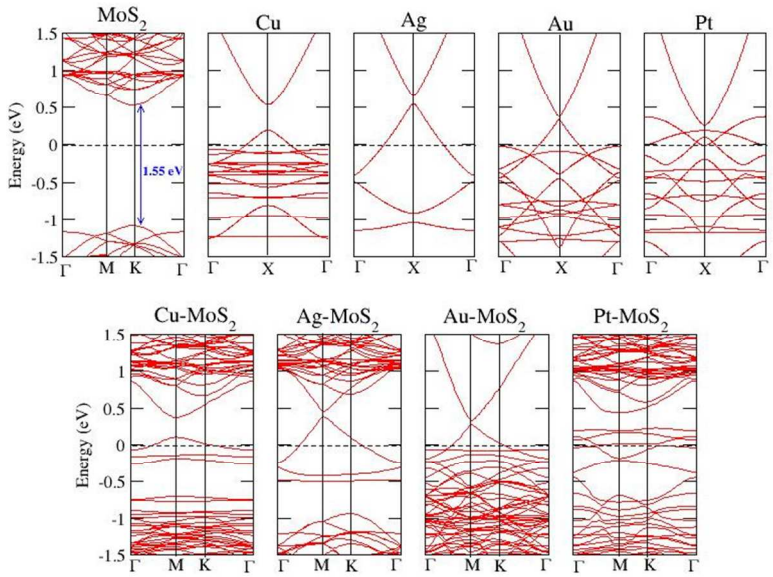

Figure 3: Electronic band structures of (top panel) the pristine monolayer and wires; and (down panel) the assembled MoS_2 monolayers.

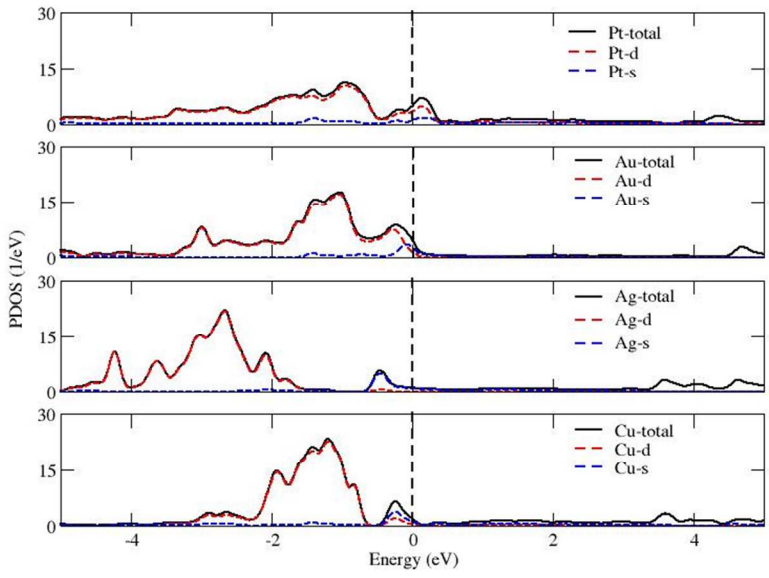

Figure 4: Projected Density of states of atomic wires for the assembled MoS_2 monolayers. Zero of the energy is aligned with Fermi energy.

Electronic band structures of the assembled monolayers and pristine wires are displayed in Fig.3. Interaction of the semiconducting MoS_2 monolayer with the metallic atomic wires dramatically modifies its electronic properties; metallic character of the assembled system appears in projected density of states in which metallic atoms of the atomic wires are associated with the electronic states near Fermi level (Fig.4). Note that the metal wires are found to retain their bands in the assembled monolayers (Fig.3). On the other hand, the pristine monolayer is semiconducting with a direct gap of 1.55 eV at K (Fig.3); top of the valance band near Fermi energy is associated with mixed Mo-d and S-p states whereas the bottom of the conduction band is mainly due to Mo-d states (see supplementary information Fig S5 [33]). This is not the case with the assembled monolayers where electronic bands at the Fermi level are partially occupied. A close examination of the valance band charge density below 0.5 eV below Fermi energy shows that the partially occupied bands are mainly associated with atoms of the metallic wires. There is small, but noticeable contribution can also be seen from Mo and S atoms in case of Cu/MoS_2 and Au/MoS_2 for the states near Fermi level (Fig. 5) which are probably responsible for the different features of valance bands below Fermi energy of Cu/MoS_2 and Au/MoS_2 assembled monolayers as compared to Ag/MoS_2 among otherwise isoelectronic configured systems. Note that appearance of overlapping spaghetti-like bands in the band structure is due to choice of a large supercell simulating the assembled monolayers in the present study, which are as a result of strong hybridization between the Mo-d, S-p and metal wire-d orbitals as can be seen in Figs. 4 and S5.

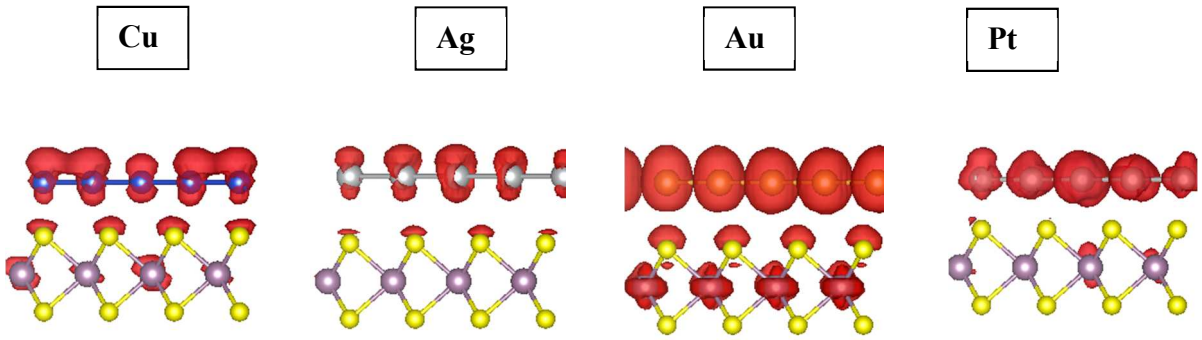

Figure 5: A side view of the valance band charge density of isosurface of 0.005 e/Å^3 below 0.5 eV Fermi level of the assembled monolayers.

The frontier orbitals of Cu, Ag and Au are s^1 d^{10} and those of Pt are s^1 d^9. This difference is reflected in Fig.3 where the d-like localized electronic states form a flat band below Fermi level and the bands crossing the Fermi level are associated with the s-like states for Cu/MoS_2, Ag/MoS_2, and Au/MoS_2. On the other hand, the partially filled d-like band crosses the Fermi level for Pt/MoS_2. Thus, the conductivity of Pt/MoS2 is likely to be dominated by the d-states of Pt wire. Considering that the intrinsic quantum ballistic conductance of a given system can be estimated by the number of bands crossing the Fermi level, the ballistic conductance for Cu/MoS_2, Ag/MoS_2, Au/MoS_2 is estimated to be $2G^0$ whereas Pt/MoS_2 appears to have the estimated conductance of $4G^0$ (Fig. 3).

3.3 Electron transport properties

Appearance of the metallic character is expected to result into the enhanced conductance of the assembled monolayer relative to the conductance expected from the semiconducting pristine monolayer. In order to quantify this enhancement, we now calculate the current-voltage (I-V) characteristics of the assembled monolayers using a model setup employed in the scanning

tunneling microscope (STM) measurements [34]. The tip is considered to be separated from the sample by a vacuum barrier width of 5 Å, mimicking a non-bonded tip configuration for the STM measurements. The cap configuration of the probe tip is modeled by a cage-like 43-atom Au cluster. The Bardin, Tersoff and Hamman (BTH) formulism[35,36] of electron tunneling was used to calculate the tunneling current in this model setup [see supplementary information-Fig. S4 [33].

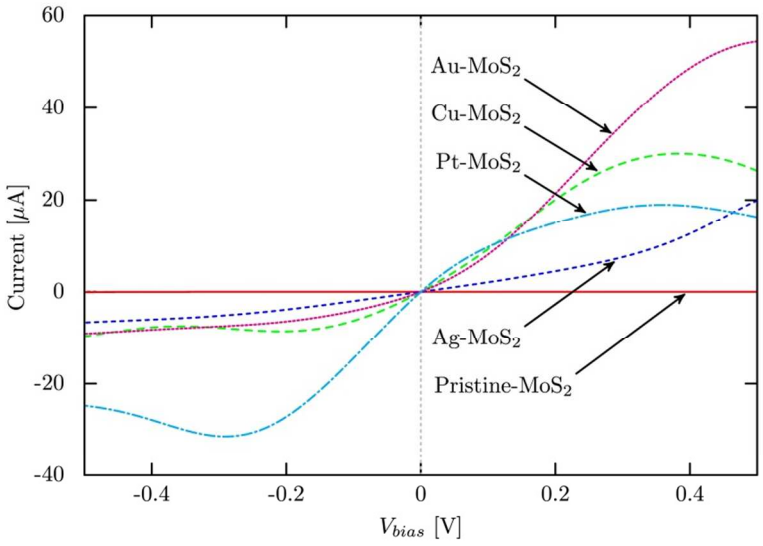

Figure 6: The current-voltage (I-V) characteristics of the pristine and assembled monolayers.

We define the bias to be positive when the sample is connected to a positive potential and electrons tunnel from the tip to the sample. It is to be noted that the tunneling current depends exponentially on the separation of the tip to sample. Therefore, the choice of tip-sample separation will determine the magnitude of the tunneling current, but should not affect the predicted trend for the assembled monolayers considered.

The calculated tunneling characteristics of the pristine and assembled monolayers are plotted in Fig.6 for the bias range of -0.5 V to +0.5V. Since the tunneling current is directly related to the convolution of the DOS of the tip and sample, appearance of finite DOS in the

vicinity of the Fermi level of the wire/MoS_2 system is likely to be cause of the increase in tunneling current with the bias voltage, V_{bias}. The pristine MoS_2 monolayer is semiconductor (Fig.6), while the assembled monolayers show ohmic-like behavior for low forward bias of ≤ 0.3 V. For the reverse bias, asymmetric characteristics appear with nearly constant current for the assembled monolayers except Pt/MoS_2. Considering that the conduction channels under an applied bias are states associated with atomic wires which are lined up near the Fermi level, difference in the current-voltage characteristics (Fig. 6) can be understood in terms of density of states of the assembled monolayers. For example, a relatively large tunneling current is seen for Au/MoS_2 as compared to that for Ag/MoS_2 for the given bias. This difference can be attributed to the significantly large occupied states (states between 0 to -0.5 V in Fig. 3) for Au/MoS_2(see supplementary information-Figure S5[33]). These states associated with atomic wires are lined up near the Fermi level and are the major tunneling "channels" under an applied bias. It is to be noted here that appearance of unoccupied states near Fermi level in Pt/MoS_2(Fig4, see supplementary information-Fig. S5[33]) results in to a large tunneling current under the reverse bias (Fig.6). Thus, the distinctly different behavior of Pt/MoS_2 with the rest of the metallic wire/MoS_2 monolayers may be attributed to distinct nature of bonding of Pt with the MoS_2 monolayer as discussed previously. It is to be noted here that electron transport across the MoS_2 monolayer coupled with Au and Ti contacts was theoretically investigated with an aim to provide guidance for the choice of metallic contacts for MoS_2-based devices [37].

4.0 Summary

In summary, the structural stability, electronic structure and electron transport properties of the metallic monoatomic wires anchored on the MoS_2 monolayer are investigated. The calculated results show the stability of the assembled monolayers with Cu, Ag, Au and Pt wires. Electronic band structure and density of states of the assembled monolayers reveal that states

associated with metallic atomic wires appear in the vicinity of Fermi level forming electron conduction channels. Cu/MoS_2, Ag/MoS_2, and Au/MoS_2 systems are found to possess $2G_0$ quantum ballistic conductance, while Pt/MoS_2 possess quantum conductance of $4G_0$ due to partially filled Pt-d states. The transverse current calculated for the assembled monolayers in the STM-like setup show significantly enhanced conduction relative to the MoS_2 pristine monolayer. Asymmetric current-voltage characteristics are predicted for the assembled monolayers except Pt/MoS_2 for which distinctly different nature of bonding is seen at the interface of the assembled monolayer. Our results unambiguously find the interaction of the MoS_2 monolayer with the metallic monoatomic wires to be relatively strong modifying its electronic properties. Cu, Ag and Au wires induce n-type doping effect whereas Pt wire induces p-type doping effect in the MoS_2 monolayer. The predicted interactions and doping effects of the monoatomic wires can be verified by experimentalists; e.g. Raman spectra [38], can reflect changes in the electronic structure induced by metal wires on the monolayer. We believe that the results of the present study are likely to extend the functionality of the MoS_2 monolayer as a candidate material for the novel applications in the areas of catalysis and optoelectronic devices. It is well known that the catalytic activity is generally attributed to the unsaturated sites or excess charge on the surface of the nanomaterial. In the case of the MoS_2 monolayer, our results shows that each S atoms have 0.3 e in excess and interaction of metal wires further induce n-type or p-type doping effect in the pristine monolayer. We therefore believe that interaction of metallic wires on MoS_2 is expected to enhance the catalytic activity especially in hydro desulfurization process.

Acknowledgements

Helpful discussions with Sanjeev K. Gupta, Xiaoliang Zhong, Mark Griep, Sankar Gowtham, Sandeep Nigam, Haiying He and Rodrigo Amorim are acknowledged. AK acknowledges the support of Michigan Tech University during his stay. RAMA and Superior, a high performance computing clusters at Michigan Technological University, were used in obtaining results presented in this paper.

References

1. Xu, M.S., et al., *Graphene-Like Two-Dimensional Materials.* Chemical Reviews, 2013. **113**(5): p. 3766-3798.
2. Wang, Q.H., et al., *Electronics and optoelectronics of two-dimensional transition metal dichalcogenides.* Nature Nanotechnology, 2012. **7**(11): p. 699-712.
3. Butler, S.Z., et al., *Progress, Challenges, and Opportunities in Two-Dimensional Materials Beyond Graphene.* Acs Nano, 2013. **7**(4): p. 2898-2926.
4. Huang, X., Z.Y. Zeng, and H. Zhang, *Metal dichalcogenide nanosheets: preparation, properties and applications.* Chemical Society Reviews, 2013. **42**(5): p. 1934-1946.
5. Song, X.F., J.L. Hu, and H.B. Zeng, *Two-dimensional semiconductors: recent progress and future perspectives.* Journal of Materials Chemistry C, 2013. **1**(17): p. 2952-2969.
6. Enyashin, A., S. Gemming, and G. Seifert, *Nanosized allotropes of molybdenum disulfide.* European Physical Journal-Special Topics, 2007. **149**: p. 103-125.
7. Kumar, A. and Ahluwalia P.K., *"Chapter 3: Tunable Electronic and Dielectric Properties of Molybdenum Disulfide" under book title 'MoS2: Materials, Physics, and Devices'*. MoS2: Materials, Physics, and Devices. Vol. 21, pp 53-76. 2014: Springer International Publishing Switzerland.
8. Myskal Sagynbaeva, P.P., Li Yunguo and M.R.a.R. Ahuja, *Tweaking the magnetism of MoS2 nanoribbon with hydrogen and carbon passivation.* Nanotechnology, 2014. **25** p. 165703.
9. Novoselov, K.S., et al., *Two-dimensional atomic crystals.* Proceedings of the National Academy of Sciences of the United States of America, 2005. **102**(30): p. 10451-10453.
10. Wilson, J. and Yoffe A.D., *The transition metal dichalcogenides discussion and interpretation of the observed optical, electrical and structural properties.* Advances in Physics, 1969. **18**(73): p. 193-335.
11. Kumar, A. and Ahluwalia P.K., *A first principle Comparative study of electronic and optical properties of 1H - MoS2 and 2H - MoS2.* Materials Chemistry and Physics, 2012. **135**(2-3): p. 755-761.
12. Mak, K.F., et al., *Atomically Thin MoS2: A New Direct-Gap Semiconductor.* Physical Review Letters, 2010. **105**(13): p. 136805.
13. Splendiani, A., et al., *Emerging Photoluminescence in Monolayer MoS2.* Nano Letters, 2010. **10**(4): p. 1271-1275.
14. Kumar, A. and Ahluwalia P.K., *Electronic structure of transition metal dichalcogenides monolayers 1H-MX2 (M = Mo, W; X = S, Se, Te) from ab-initio theory: new direct band gap semiconductors.* European Physical Journal B, 2012. **85**(6): p. 186.
15. Kumar, A. and P.K. Ahluwalia , *Tunable dielectric response of transition metals dichalcogenides MX2 (M=Mo, W; X=S, Se, Te): Effect of quantum confinement.* Physica B-Condensed Matter, 2012. **407**(24): p. 4627-4634.
16. Kumar, A. and Ahluwalia P.K., *Semiconductor to metal transition in bilayer transition metals dichalcogenides MX2 (M = Mo, W; X = S, Se, Te).* Modelling and Simulation in Materials Science and Engineering, 2013. **21**(6): p. 065015.
17. Kumar, A. and Ahluwalia P.K., *Mechanical strain dependent electronic and dielectric properties of two-dimensional honeycomb structures of MoX2 (X=S, Se, Te).* Physica B-Condensed Matter, 2013. **419**: p. 66-75.
18. Radisavljevic, B., et al., *Single-layer MoS2 transistors.* Nature Nanotechnology, 2011. **6**(3): p. 147-150.
19. Li, H., et al., *Fabrication of Single- and Multilayer MoS2 Film-Based Field-Effect Transistors for Sensing NO at Room Temperature.* Small, 2012. **8**(1): p. 63-67.
20. He, Q.Y., et al., *Fabrication of Flexible MoS2 Thin-Film Transistor Arrays for Practical Gas-Sensing Applications.* Small, 2012. **8**(19): p. 2994-2999.
21. Chen, J., et al., *Highly Conductive and Flexible Paper of 1D Silver-Nanowire-Doped Graphene.* Acs Applied Materials & Interfaces, 2013. **5**(4): p. 1408-1413.

22. Sreeprasad, T.S., et al., *Controlled, Defect-Guided, Metal-Nanoparticle Incorporation onto MoS_2 via Chemical and Microwave Routes: Electrical, Therrmal, and Structural Properties.* Nano Letters, 2013. **12**(9): p. 4434-41.
23. Shi Y., Huang J.-K., Jin L., Hsu Y-T, Yu S. F., Li L.-J., and Yang H. Y., *Selective Decoration of Au Nanoparticles on Monolayer MoS_2 Single Crystals*, Scientific Reports 2013. **3** (5) p 01839
24. Huang J., Dong Z., Li Y., Li J., Tang W., Yang H., Wang J.,Bao Y., Jin J., Li R.,*MoS_2 nanosheet functionalized with Cu nanoparticles and its application for glucose detection*, Materials Research Bulletin, 2013. **48** (11), p. 4544–4547.
25. Zhao J., Yang S.,Zheng H., Li Y., *Facile synthesis of MoS_2 nanosheet-silver nanoparticles composite for surface enhanced Raman scattering and electrochemical activity*, Journal of Alloys and Compounds, 2013. **559** (5), p. 87–91.
26. Yanson, A.I., et al., *Formation and manipulation of a metallic wire of single gold atoms.* Nature, 1998. **395**(6704): p. 783-785.
27. Hong, B.H., et al., *Ultrathin single-crystalline silver nanowire arrays formed in an ambient solution phase.* Science, 2001. **294**(5541): p. 348-351.
28. Agrait, N., A.L. Yeyati, and J.M. van Ruitenbeek, *Quantum properties of atomic-sized conductors.* Physics Reports-Review Section of Physics Letters, 2003. **377**(2-3): p. 81-279.
29. Smit, R.H.M., et al., *Common origin for surface reconstruction and the formation of chains of metal atoms.* Physical Review Letters, 2001. **87**(26): p. 266102.
30. Troullier, N. and J.L. Martins, *Efficient Pseudopotentials for Plane-Wave Calculations .2. Operators for Fast Iterative Diagonalization.* Physical Review B, 1991. **43**(11): p. 8861-8869.
31. Soler, J.M., et al., *The SIESTA method for ab initio order-N materials simulation.* Journal of Physics-Condensed Matter, 2002. **14**(11): p. 2745-2779.
32. Zarechnaya E.Yu., Skorodumova N.V., Simak S.I., Johansson B., , Isaev E.I., *Theoretical study of linear monoatomic nanowires, dimer and bulk of Cu, Ag, Au, Ni, Pd and Pt,* Computational Materials Science 2008. **43**:p. 522–530.
33. Provided as supplementary information.
34. Gupta, S.K., et al., *Electron tunneling characterstics of a cubic quantum dot, $(PbS)_{32}$.* The Journal of Chemical Physics, 2013. **139:** p. 244307.
35. Tersoff, J. and D.R. Hamann, *Theory and Application for the Scanning Tunneling Microscope.* Physical Review Letters, 1983. **50**(25): p. 1998-2001.
36. Tersoff, J. and D.R. Hamann, *Theory of the Scanning Tunneling Microscope.* Physical Review B, 1985. **31**(2): p. 805-813.
37. Bai Z., Markussen T., and Thygesen K. S., arXiv:1311.2393v1, 11 Nov 2013.
38. Rao B. G., Matte H. S. S. R., Rao C. N. R., Decoration of Few-Layer Graphene-Like MoS_2 and $MoSe_2$ by Noble Metal Nanoparticles, Journal of Cluster Science, 2012. 23 (3), p 929-937.